Pore translocation of knotted polymer chains: how friction depends on knot complexity

A. Suma[1], A. Rosa[1], C. Micheletti[1*]
[1] *SISSA, International School for Advanced Studies, via Bonomea 265, I-34136 Trieste, Italy*

Knots can affect the capability of polymers to translocate through narrow pores in complex and counter-intuitive ways that are still relatively unexplored. We report here on a systematic theoretical and computational investigation of the driven translocation of flexible chains accommodating a large repertoire of knots trapped at the pore entrance. These include composites knots, which are the most common form of spontaneous entanglement in long polymers. Two unexpected results emerge from this study. First, the high force translocation compliance does not decrease systematically with knot complexity. Secondly, the response of composite knots is so dependent on the order of their factor knots, that their hindrance can even be lower than some of their prime components. We show that the resulting rich and seemingly disparate phenomenology can be captured in a seamless framework based on the mechanism by which tension is propagated along and past the knots. The quantitative scheme can be viably used for predictive purposes and hence ought to be useful in applicative contexts, too.

The driven translocation of linear polymers through narrow pores is increasingly investigated for its relevance in polymer physics, molecular biology and single-molecule experiments, including genome sequencing[1–18]. In all these contexts, a key issue emerging from theoretical and experimental studies is how the translocation compliance of a chain is affected by physical knots which are too cumbersome to pass through the pore [19–22]. This question is relevant both for general polymer physics, because knots and other forms of entanglement abound in chains that are sufficiently long or densely packed[23–29] and, in particular, for the manipulation or *in vivo* processing of biopolymers, where either of these two conditions are usually met [30–33].

For the reference case of an unknotted chain, the average time, τ, required to translocate it through a narrow pore typically scales as $\tau \propto N^{1+\nu}/f$ [2, 4, 6], where f is the dragging force, N is the number of chain monomers and ν is the Flory critical exponent for the bulk radius of gyration, $R_g \sim N^{\nu}$. Notably, the proportionality of τ and f breaks down if even the simplest knot types are present in the chain [20]. This occurs because of the substantial friction developed between contacting monomers in the knotted region[9, 34] which, once trapped and tightened at the pore entrance hinders, partially or completely, the sliding of the chain along its knotted contour.

Here, to advance the current understanding of this problem, we address the general and yet still unexplored issue of how the translocation compliance of a knotted chain depends on the complexity of its entanglement.

Inspired by the eletrophoretic driven translocation of polyeletrolytes through nanopores [12–14, 18, 35–38] we model the translocating polymer as a flexible chain of beads with screened electrostatic self-repulsion. Specifically we considered chains of $N = 15,000$ identical beads of diameter σ and charge q. The chain internal energy, $\mathcal{H}$ consists of a FENE potential providing the chain connectivity[39], a Debye-Hückel electrostatic interaction with screening length λ_{DH} and a truncated and shifted Lennard-Jones potential for the excluded volume effects. Setting the typical energy scale, ϵ, equal to the system thermal energy, $\epsilon = \kappa_B T$, $\mathcal{H}$ is written as:

$$\mathcal{H} = -\sum_{i=1}^{N-1} \frac{KR_0^2}{2} \ln[1 - \frac{d_{i,i+1}^2}{R_0^2}] + \sum_{\substack{i,j \\ j>i+1}}^{N} \epsilon \frac{l_B}{d_{i,j}} (\frac{q}{e})^2 e^{-\frac{d_{i,j}}{\lambda_{DH}}}$$

$$+ \sum_{i,j;j>i}^{N} \left[4\epsilon_{i,j}\left[\left(\frac{\sigma}{d_{i,j}}\right)^{12} - \left(\frac{\sigma}{d_{i,j}}\right)^{6}\right] + \epsilon_{i,j}\right]\theta(2^{1/6}\sigma - d_{i,j})$$

where $d_{i,j}$ is the distance of beads i and j, $K = 70\epsilon/\sigma$, $R_0 = 1.5\sigma$ is the maximum bond length, l_B is the Bjerrum length, e is the electron charge, $\epsilon_{i,j}$ is equal to 2.33ϵ for consecutive beads ($j = i \pm 1$) and simply equal to ϵ otherwise and θ is the Heaviside function. Analogously to ref. [20], typical operating conditions are matched by setting $T = 300$K, $q/e = 1.5$, $l_B = 0.7\sigma$, $\lambda_{DH} = 0.9\sigma$ and by fixing the nanopore nominal diameter and longitudinal span equal to 1.55σ and 10σ, respectively[40, 41]. The pore is embedded in an impenetrable slab separating the *cis* and *trans* regions, see Fig. 1a, and is narrow enough to prevent the passage of physical knots. The translocation is driven by a uniform longitudinal electric field active only within the pore and which pulls each bead inside it with a force f.

As clarified in ref. [20] the translocation process of equilibrated chains accommodating the simplest knot type (the 3_1 or trefoil knot) proceeds at the same rate of unknotted chains up to when the knotted region is dragged to the pore entrance. After this transient, the tightening of the knot produces a sliding friction which causes the

*To whom correspondence should be addressed:
cristian.micheletti@sissa.it

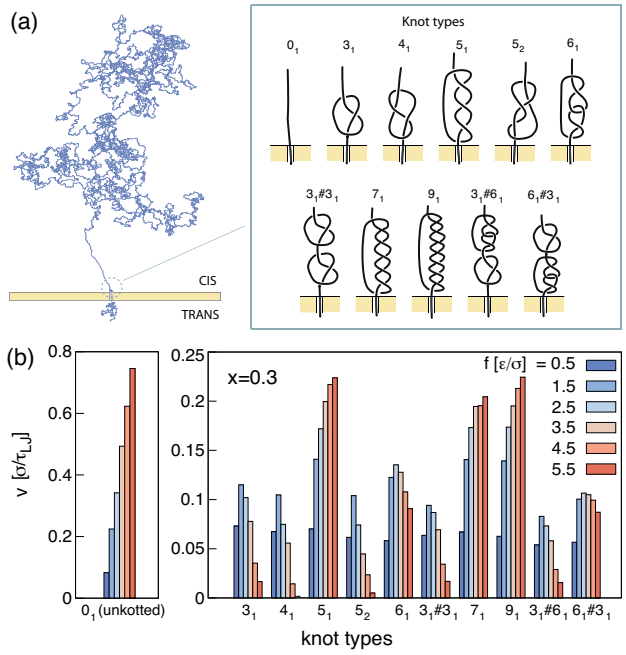

FIG. 1: (a) Snapshot of an early stage of translocation of a knotted chain. Inset: repertoire of knots prepositioned at the pore entrance. (b) Average translocation speed, v, measured, at 30% translocated fraction, for various applied forces, f. Across all topologies the estimated relative error on v is 5% on average and never larger than 8%.

translocation to slow down and even stall at sufficiently high driving forces, see SI.

For an equal footing comparison of the translocation compliance of differently knotted chains, we neglect the aforementioned transient, whose duration varies according to the knot positioning along the chain, and focus on how the system evolution after the knot has tightened at the pore entrance. To do so we prepositioned inside the pore a short lead, up to 100-beads long, spanning the whole channel and with its *cis* terminus tied in various types of knots. The free knot end was finally connected to the terminal of an equilibrated unknotted chain. The system was evolved with a constant-temperature Langevin dynamics integrated numerically with the LAMMPS simulation package[42]. For a given topology of the lead, observables were averaged over at least five runs started from independent configurations of the attached equilibrated chain; see SI for further model and methodological details.

The considered repertoire of knots is sketched in Fig 1a and extends significantly beyond the 3_1 and 4_1 instances considered before. The set is ordered for increasing nominal complexity, i.e. the number of crossings in the minimal two-dimensional projection, that is generally a key determinant of topological friction [9, 43–50]. In particular, the repertoire of knots includes a sizable number of representatives from the two main topological families of simple prime knots: twist knots, which can be unknotted by a single strand passage at a clasp point, and torus knots, which can be drawn as closed curves on the surfaces of a torus. The former group includes the 3_1, 4_1, 5_2 and 6_1 knots, while the latter consists of the 3_1, 5_1, 7_1 and 9_1; notice that the 3_1 knot appears, exceptionally, in both groups. In addition, we consider composite knots resulting from the serial addition of prime knots. We recall that composite knots are the most common form of entanglement in sufficiently long chains[51].

The translocation compliance across the knots repertoire was studied for values of f in the 0.5–8 ϵ/σ range, placing the total pulling force in the high stretching regime, see SI. The results are shown in Fig. 1b and pertain to the average translocation velocity, v, measured at $x = 0.3$, with x being the chain fraction already passed through the pore. Equivalent results, apart from a rescaling factor, are obtained using different x thresholds, see SI. The reference case of unknotted chains is shown in a separate panel of Fig. 1b because of its wider range of velocities. For such case, v has the expected linear dependence on f at fixed x [2].

By contrast, the knotted chain translocation speed presents several unexpected tiers of complexity upon varying both the applied force and the knot type.

First, at any of the considered forces, the average velocities do not systematically decrease with knot complexity. Secondly, only few of the prime knots display the non-monotonic v versus f dependence signalling the onset of jamming. These are knots belonging to the twist family. Even increasing the force applied to each of the ~ 10 beads in the channel up to $f \sim 8\epsilon/\sigma$, the largest that FENE bonds can withstand in the simulation protocol, the onset of jamming is not seen for the 5_1, 7_1 and 9_1 torus knots. To our knowledge, this interesting qualitative dicotomy has been previously found only in a specific context, namely for low- or moderately- tensioned knotted chains in a surrounding fluid (with 3_1 knot behaving as a torus rather than as a twist knot) [48, 50]. In these cases torus and twist knots still have comparable mobilities, while here their high-force translocation velocities can vary by an order of magnitude, see Fig. 1b.

Finally, the translocation behaviour of compositely-knotted chains is unexpectedly rich and intriguing, too. In fact, their hindrance can be comparable and even lower than for chains hosting only one of their components, see e.g. $3_1\#3_1$ vs 3_1 and $6_1\#3_1$ vs 3_1, and it is distinctly non-commutative in the knots order, see $6_1\#3_1$ vs $3_1\#6_1$.

These intriguing and seemingly disparate properties can be quantitatively accounted for by a seamless framework based on how the driving force is propagated along and past the knot trapped at the pore entrance.

Following the spirit of the Euler-Eytelwein analysis of tension and friction in a rope wound around a capstan [52] we profile the relationship between the chain tension measured immediately before and after the knot (or

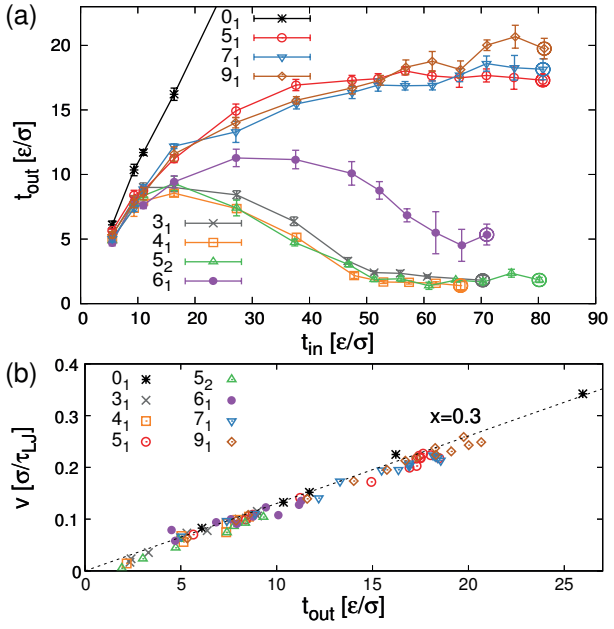

FIG. 2: (a) Average chain tensions at the beginning (t_{in}) and end (t_{out}) of various prime knots. Beyond the circled data points chain breaks occur systematically. (b) Translocation speed at 30% translocated fraction versus t_{out} for all considered prime knots.

simply before and after the pore for unknotted chains). These two key quantities will be denoted with t_{in} and t_{out} respectively. The former is obtained by multiplying f by the average number, $n \sim 10$, of beads in the pore: $t_{in} = n\,f$, while t_{out} is measured directly. Specifically, as detailed in the SI, the tension of the bond connecting beads i and $i+1$ is obtained by computing the tangential component of the total force on bead i minus the bonding one with bead $i+1$.

The relationship between t_{in} and t_{out} is shown in Fig. 2a for all considered prime knots. The significant reduction of chain tension operated by any of the prime knots vividly emerges from the comparison with the unknotted case. More important, however, is the substantial spread of the output tension across the knots repertoire. This heterogeneity originates from the very diverse response of torus knots from twist ones. It is clearly the latter that produce the largest topological friction and, due to the rapid decrease of t_{out} with t_{in}, can eventually halt the translocation process at the largest applied forces, unlike torus knots.

The tension response curves, which to our knowledge have not been previously introduced in this context, are key to characterize the varied behaviour of prime knots in Fig. 2a, and to predict that of composite ones.

To this end we note that the complex translocation phenomenology across all knots in Fig. 2a is underpinned by a simple linear relationship between v and t_{out}, see Fig. 1b. Notice that the data include the case of unknotted chains too. Therefore, the behaviour of chains accommodating very different knots is practically equivalent to that of an entanglement-free chain translocated by a total force equal to t_{out}.

The detailed mechanisms governing the dissipative transmission of tension along the knot contour can be gleaned from the bond strain profiles of the chain portion near the pore. Typical examples are shown in Fig. 3a and additional ones are provided as SI. Compared to the smoothly decreasing strain of the unknotted case, the strain profile is riddled with peaks in the knotted region and falls to negligible values immediately outside it. Unlike equilibrated chains pulled at both termini[53], the peaks profile is noticeably asymmetrical with respect to the knot midpoint, with the highest strain occuring almost invariably at the pore entrance.

Considering that the bond strain reflects the chain self-friction along the knot contour, one may envisage that the largest dissipation of the input tension should occur at the point with the highest strain.

This is confirmed by Fig. 3b where the topological friction, as captured by the tension transmission coefficient, $r \equiv t_{out}/t_{in}$, is plotted against the maximum (peak) bond extension, d_{max}. Again, the behaviour of torus and twist knots are neatly separated, and the dispersion within either of the two families is much reduced compared to Fig. 2a.

Mapping out the strain peaks on the actual conformations of the tightened knots clarifies the origin of the major difference between torus and twist knots. As exemplified by the snapshots shown in Fig. 3a, torus knots have a single region, namely the knot entrance, where the strain peaks overcome the reference profile of the unknotted case. Twist knots instead have two distinct regions: the knot entrance plus the exit.

This suggests that the much higher hindrance offered by twist knots results from the combination of two distinct dissipative mechanisms, as opposed to the single one of torus knots.

To verify this hypothesis we parametrize the functional dependence of the tension reduction ratio of torus knots, r versus d_{max}, see dashed line in Fig. 3b, and used it to predict the tension drop of twist knots. Specifically, we assumed for simplicity that the two distinct friction regions are independent and acting as the single friction point of torus knots. Accordingly, the predicted tension reduction of twist knots is given by the multiplicative composition of the individual frictional effects: $r_{pred} \equiv r(d_1) \cdot r(d_2)$ where d_1 and d_2 are the peak bond elongations at the knot entrance and exit.

As shown by Fig. 3c, the predicted tension reduction is in very good agreement with the measured one. We note that the predictions are practically deterministic, since no tunable parameter is involved. This further supports the use of the tension reduction at highly-strained points as the dominant mechanism for capturing and unifying

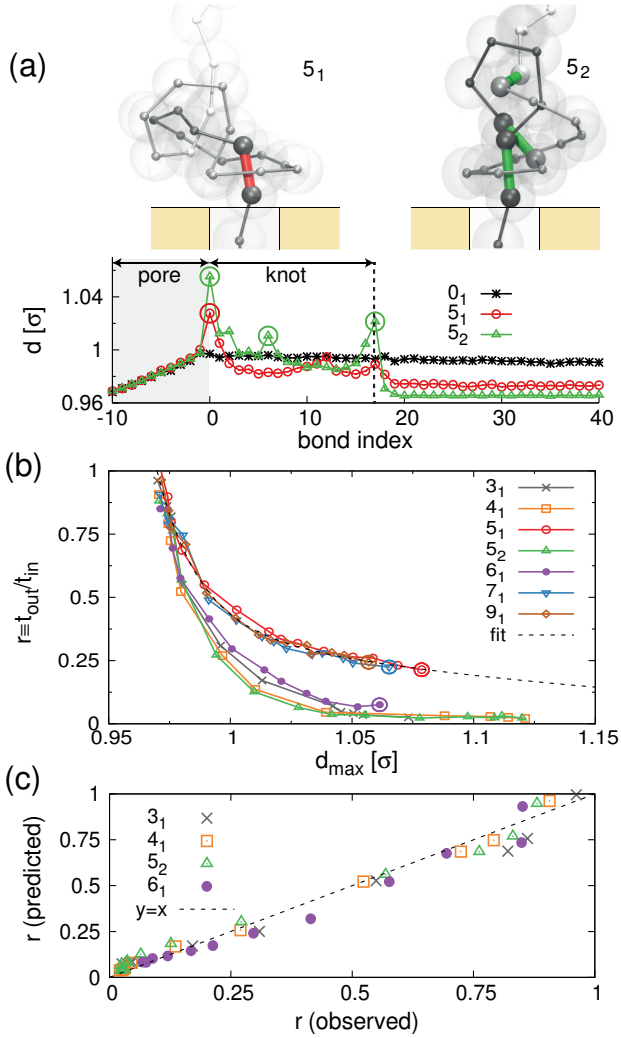

FIG. 3: (a) Profile of the average length, d, of chain bonds proximal to the pore for three types of knotted chains pulled at $f = 5.5$; index zero denotes the first *cis* bond. Bonds with the peak elongation (circled) are highlighted in the snapshots. (b) Tension transmission ratio, $r \equiv t_{out}/t_{in}$, versus the maximum bond length, d_{max}. The dashed line is the fit of the torus knots data points using, empirically, a double-exponential: $r(d) = 0.57\exp[-(d - d^0)/0.017] + 0.39\exp[-(d - d^0)/0.18]$ with $d^0 = 0.97$. (c) Predicted versus measured tension ratio for twist knots.

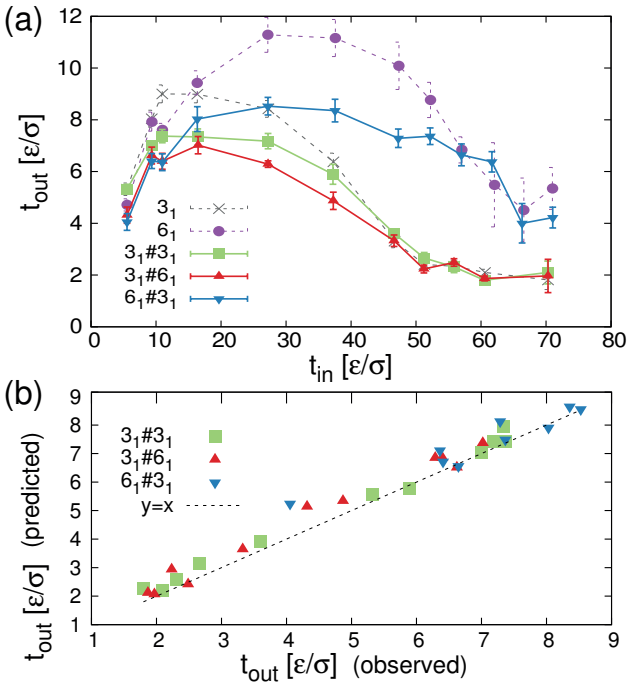

FIG. 4: (a) Average chain tensions at the beginning, t_{in}, and end, t_{out}, of composites knots and their components. (b) Predicted versus measured output tension for these knots.

the observed disparate phenomenology of Fig. 1b.

Indeed, the same concept can be used to predict, and hence rationalize the two key features of the overall hindrance offered by composite knots, namely that it can be smaller than that of their individual components and that it is non-commutative, see Fig. 1b.

In fact, both aspects emerge from the analysis of the peak strain analysis or equivalently, and perhaps more simply, that of the tension response curves of prime knots shown in Fig. 2a. Specifically, the same concepts used for the predictions in Fig. 3 can be transferred here by assuming that the output tension of composite knots, shown in Fig. 4a, results from the multiplicative combination of the frictional effects of the prime components. For instance, for given f (and hence t_{in}) the predicted output tension of the $3_1\#6_1$ knot is obtained by using the curves in Fig. 2a to (*i*) establish the tension $t_{out,3_1}$ immediately past the first knot, then (*ii*) using it as t_{in} for the 6_1 component, and finally computing the corresponding t_{out}, which yields the predicted output tension. Notice that this scheme is intrinsically non-commutative and hence has *a priori* the potential to account for both of the aforementioned effects. Indeed, the predicted output tensions are in very good agreement with the actual measurements for all considered composite knots, see Fig. 4b. We emphasize that the predictions are based only on a spline interpolation of the data in Fig. 2a with no free adjustable parameters.

In conclusion, we have shown that the complex and varied phenomenology of knotted chains translocation can be seamlessly captured in a transparent, quantitative framework based on the mechanism by which tension is propagated along and past the knots. This scheme, here studied for a generic polyelectrolyte model, ought to be useful in applicative contexts such as nanopore translocation of nucleic acids filaments [12–14, 18, 35–38], especially the flexible single-stranded ones. In particular, it could be useful for inferring the general topology of chains based on their translocation response or for har-

nessing their topological friction to optimally reduce and control their translocation speed.

Acknowledgement

We thank G. Bussi, M. Caraglio, A. McGown and G. Polles for valuable discussions. We acknowledge support from the Italian Ministry of Education grant PRIN 2010HXAW77.

Supporting Information Available

Supporting Information: Further details of the model, system setup and translocation properties; chain tension, strain and length of the knotted region.

[1] Chuang, J.; Kantor, Y.; Kardar, M. Anomalous dynamics of translocation. *Phys. Rev. E* **2001**, *65*, 011802.

[2] Kantor, Y.; Kardar, M. Anomalous dynamics of forced translocation. *Phys. Rev. E* **2004**, *69*, 021806.

[3] Reisner, W.; Morton, K. J.; Riehn, R.; Wang, Y. M.; Yu, Z.; Rosen, M.; Sturm, J. C.; Chou, S. Y.; Frey, E.; Austin, R. H. Statics and Dynamics of Single DNA Molecules Confined in Nanochannels. *Phys. Rev. Lett.* **2005**, *94*, 196101.

[4] Grosberg, A. Y.; Nechaev, S.; Tamm, M.; Vasilyev, O. How long does it take to pull an ideal polymer into a small hole? *Phys. Rev. Lett.* **2006**, *96*, 228105.

[5] Muthukumar, M. Mechanism of DNA transport through pores. *Annu. Rev. Biophys. Biomol. Struct.* **2007**, *36*, 435–450.

[6] Chatelain, C.; Kantor, Y.; Kardar, M. Probability distributions for polymer translocation. *Phys. Rev. E* **2008**, *78*, 021129.

[7] Palyulin, V. V.; Ala-Nissila, T.; Metzler, R. Polymer translocation: the first two decades and the recent diversification. *Soft Matter* **2014**, *10*, 9016–9037.

[8] Reinhart, W. F.; Reifenberger, J. G.; Gupta, D.; Muralidhar, A.; Sheats, J.; Cao, H.; Dorfman, K. D. Distribution of distances between DNA barcode labels in nanochannels close to the persistence length. *J. Chem. Phys.* **2015**, *142*, 064902.

[9] Huang, L.; Makarov, D. E. Translocation of a knotted polypeptide through a pore. *J. Chem. Phys.* **2008**, *129*, 121107–121107.

[10] Luan, B.; Aksimentiev, A. Electro-osmotic screening of the DNA charge in a nanopore. *Phys. Rev. E* **2008**, *78*, 021912.

[11] Plesa, C.; Kowalczyk, S. W.; Zinsmeester, R.; Grosberg, A. Y.; Rabin, Y.; Dekker, C. Fast translocation of proteins through solid state nanopores. *Nano letters* **2013**, *13*, 658–663.

[12] Schneider, G. F.; Dekker, C. DNA sequencing with nanopores. *Nat. Nanotechnol.* **2012**, *30*, 326–328.

[13] Zwolak, M.; Di Ventra, M. Physical approaches to DNA sequencing and detection. *Rev. Mod. Phys.* **2008**, *80*, 141.

[14] Branton, D. et al. The potential and challenges of nanopore sequencing. *Nat. Biotechnol.* **2008**, *26*, 1146.

[15] van Dorp, S.; Keyser, U. F.; Dekker, N. H.; Dekker, C.; Lemay, S. G. Origin of the electrophoretic force on DNA in solid-state nanopores. *Nat. Phys.* **2009**, *5*, 347.

[16] Kravats, A.; Jayasinghe, M.; Stan, G. Unfolding and translocation pathway of substrate protein controlled by structure in repetitive allosteric cycles of the ClpY ATPase. *Proc. Natl. Acad. Sci. USA* **2011**, *108*, 2234–2239.

[17] Larkin, J.; Henley, R. Y.; Muthukumar, M.; Rosenstein, J. K.; Wanunu, M. High-bandwidth protein analysis using solid-state nanopores. *Biophys. J .* **2014**, *106*, 696–704.

[18] Plesa, C.; Verschueren, D.; Ruitenberg, J. W.; Witteveen, M. J.; Jonsson, M. P.; Grosberg, A. Y.; Rabin, Y.; Dekker, C. Observation of DNA Knots Using Solid-State Nanopores. *Biophys. J.* **2015**, *108*, 166a.

[19] Matthews, R.; Louis, A. A.; Yeomans, J. M. Knot-Controlled Ejection of a Polymer from a Virus Capsid. *Phys. Rev. Lett.* **2009**, *102*, 088101.

[20] Rosa, A.; Di Ventra, M.; Micheletti, C. Topological jamming of spontaneously knotted polyelectrolyte chains driven through a nanopore. *Phys. Rev. Lett.* **2012**, *109*, 118301.

[21] Szymczak, P. Translocation of Knotted Proteins into Mitochondria. *Biophys. J.* **2013**, *104*, 301a.

[22] Marenduzzo, D.; Micheletti, C.; Orlandini, E.; Sumners, D. W. Topological friction strongly affects viral DNA ejection. *Proc. Natl. Acad. Sci. USA* **2013**, *110*, 20081–20086.

[23] Sumners, D. W.; Whittington, S. G. Knots in self-avoiding walks. *J. Phys. A: Math. Gen.* **1988**, *21*, 1689–1694.

[24] Michels, J.; Wiegel, F. The distribution of the Alexander polynomials of knots confined to a thin layer. *J. Phys. A: Math. Gen.* **1989**, *22*, 2393–2398.

[25] Shimamura, M. K.; Deguchi, T. Knot complexity and the probability of random knotting. *Phys. Rev. E* **2002**, *66*, 040801.

[26] Arsuaga, J., et al. Knotting probability of DNA molecules confined in restricted volumes: DNA knotting in phage capsids. *Proc. Natl. Acad. Sci. USA* **2002**, *99*, 5373.

[27] Virnau, P.; Kantor, Y.; Kardar, M. Knots in globule and coil phases of a model polyethylene. *J. Am. Chem. Soc.* **2005**, *127*, 15102.

[28] Michieletto, D.; Marenduzzo, D.; Orlandini, E.; Alexander, G. P.; Turner, M. S. Threading Dynamics of Ring Polymers in a Gel. *ACS Macro Letters* **2014**, *3*, 255–259.

[29] Lo, W.-C.; Turner, M. S. The topological glass in ring polymers. *Europhysics Letters* **2013**, *102*, 58005.

[30] Meluzzi, D.; Smith, D. E.; Arya, G. Biophysics of knotting. *Annu. Rev. Biophys.* **2010**, *39*, 349–366.

[31] Marenduzzo, D.; Micheletti, C.; Orlandini, E. Biopolymer organization upon confinement. *J. Phys. Condens. Matter* **2010**, *22*, 283102.

[32] Virnau, P.; Mallam, A.; Jackson, S. Structures and folding pathways of topologically knotted proteins. *J. Phys. Condens. matter* **2011**, *23*, 033101.

[33] Poier, P.; Likos, C. N.; Matthews, R. Influence of Rigidity and Knot Complexity on the Knotting of Confined Polymers. *Macromolecules* **2014**, *47*, 3394–3400.

[34] Kirmizialtin, S.; Makarov, D. E. Simulations of the untying of molecular friction knots between individual polymer strands. *J Chem Phys* **2008**, *128*, 094901.

[35] Lagerqvist, J.; Zwolak, M.; Di Ventra, M. Fast DNA Sequencing via Transverse Electronic Transport. *Nano Lett.* **2006**, *6*, 779–782.

[36] Ohshiro, T.; Matsubara, K.; Tsutsui, M.; Furuhashi, M.; Taniguchi, M.; Kawai, T. Single-molecule electrical random resequencing of DNA and RNA. *Sci. Rep.* **2012**, *2*,

501.

[37] He, Y.; Tsutsui, M.; Scheicher, R. H.; Bai, F.; Taniguchi, M.; Kawai, T. Thermophoretic manipulation of DNA translocation through nanopores. *ACS nano* **2013**, *7*, 538–546.

[38] Rahong, S.; Yasui, T.; Yanagida, T.; Nagashima, K.; Kanai, M.; Meng, G.; He, Y.; Zhuge, F.; Kaji, N.; Kawai, T.; Baba, Y. Self-assembled nanowire arrays as three-dimensional nanopores for filtration of DNA molecules. *An. Sci.* **2015**, *31*, 153–157.

[39] Kremer, K.; Grest, G. S. Dynamics of entangled linear polymer melts: A molecular-dynamics simulation. *J. Chem. Phys.* **1990**, *92*, 5057.

[40] Derrington, I. M., et al. Nanopore DNA sequencing with MspA. *Proc. Natl. Acad. Sci. USA* **2010**, *107*, 16060.

[41] Maffeo, C.; Schöpflin, R.; Brutzer, H.; Stehr, R.; Aksimentiev, A.; Wedemann, G.; Seidel, R. DNA-DNA interactions in tight supercoils are described by a small effective charge density. *Phys. Rev. Lett.* **2010**, *105*, 158101.

[42] Plimpton, S. Fast parallel algorithms for short range molecular dynamics. *J. Comp. Phys.* **1995**, *117*, 119.

[43] Bao, X. R.; Lee, H. J.; Quake, S. R. Behavior of Complex Knots in Single DNA Molecules. *Phys. Rev. Lett.* **2003**, *91*, 265506.

[44] Huang, L.; Makarov, D. E. Langevin Dynamics Simulations of the Diffusion of Molecular Knots in Tensioned Polymer Chains. *J. Phys. Chem. A* **2007**, *111*, 10338–10344.

[45] Metzler, R.; Reisner, W.; Riehn, R.; Austin, R.; Tegenfeldt, J. O.; Sokolov, I. M. Diffusion mechanisms of localised knots along a polymer. *Europhysics Letters* **2006**, *76*, 696.

[46] Dommersnes, P. G.; Kantor, Y.; Kardar, M. Knots in charged polymers. *Phys. Rev. E* **2002**, *66*, 031802.

[47] Vologodskii, A. Brownian Dynamics Simulation of Knot Diffusion along a Stretched DNA Molecule. *Biophys. J.* **2006**, *90*, 1594.

[48] Matthews, R.; Louis, A. A.; Yeomans, J. M. Effect of topology on dynamics of knots in polymers under tension. *Europhys. Lett.* **2010**, *89*, 20001.

[49] Di Stefano, M.; Tubiana, L.; Di Ventra, M.; Micheletti, C. Driving knots on DNA with AC/DC electric fields: topological friction and memory effects. *Soft Matter* **2014**, *10*, 6491–6498.

[50] Renner, C. B.; Doyle, P. S. Untying Knotted DNA with Elongational Flows. *ACS Macro Letters* **2014**, *3*, 963–967.

[51] Micheletti, C.; Marenduzzo, D.; Orlandini, E. Polymers with spatial or topological constraints: Theoretical and computational results. *Phys. Reports* **2011**, *504*, 1.

[52] Konyukhov, A.; Schweizerhof, K. *Computational Contact Mechanics*; Springer: Berlin, 2013.

[53] Saitta, A. M.; Soper, P. D.; Wasserman, E.; Klein, M. L. Influence of a knot on the strength of a polymer strand. *Nature* **1999**, *399*, 46.